

Article

One-Dimensional Fluorene-Based Co(II) Phosphonate $\text{Co}(\text{H}_2\text{O})_2\text{PO}_3\text{C}-\text{C}_{12}\text{H}_9\cdot\text{H}_2\text{O}$: Structure and Magnetism

Clarisse Bloyet ¹ , Jean-Michel Rueff ^{1,*}, Olivier Perez ¹, Alain Pautrat ¹, Vincent Caignaert ¹, Bernard Raveau ^{1,*}, Guillaume Rogez ² and Paul-Alain Jaffrès ³

¹ Normandie Univ, ENSICAEN, UNICAEN, CNRS, CRISMAT, 14000 Caen, France; clarisse.bloyet@ensicaen.fr (C.B.); olivier.perez@ensicaen.fr (O.P.); alain.pautrat@ensicaen.fr (A.P.); vincent.caignaert@ensicaen.fr (V.C.)

² IPCMS, UMR Unistra-CNRS 7504, 23 rue du Loess, BP 43, 67034 Strasbourg CEDEX 2, France; Guillaume.Rogez@ipcms.unistra.fr

³ CEMCA UMR CNRS 6521, Université de Brest, IBSAM, 6 Avenue Victor Le Gorgeu, 29238 Brest, France; Paul-Alain.Jaffres@univ-brest.fr

* Correspondence: jean-michel.rueff@ensicaen.fr (J.-M.R.); bernard.raveau@ensicaen.fr (B.R.)

Received: 4 July 2018; Accepted: 3 September 2018; Published: 5 September 2018



Abstract: A new Co(II) phosphonate, $\text{Co}(\text{H}_2\text{O})_2\text{PO}_3\text{C}-\text{C}_{12}\text{H}_9\cdot\text{H}_2\text{O}$, has been synthesized under hydrothermal conditions. The monoclinic $P2_1/c$ structure of this organic–inorganic hybrid consists of isolated perovskite-type chains of corner-shared $\text{CoO}_4(\text{H}_2\text{O})_2$ octahedra interconnected via phosphonate groups. The unique one-dimensional structure of this phase is closely related to the single-chain magnet (SCM) phosphonate $\text{Co}(\text{H}_2\text{L})(\text{H}_2\text{O})$, with $\text{L} = 4\text{-Me-C}_6\text{H}_4\text{-CH}_2\text{N}(\text{CPO}_3\text{H}_2)_2$, that contains isolated chains of CoO_5N octahedra. Like the latter, this hybrid exhibits 1D antiferromagnetic interactions and the possibility of an effective pseudo spin contribution due to spin canting at low temperature, but, in contrast, is not an SCM. This different magnetic behavior is explained by the different geometry of the octahedral chains and by the possible existence of weak antiferromagnetic interactions between the chains. This opens the route to the investigation of a large series of compounds by tuning the chemical composition and structure of the phosphonic acid used as organic precursor of hybrid materials.

Keywords: cobalt phosphonate; 1D hybrid; fluorene; spin canting

1. Introduction

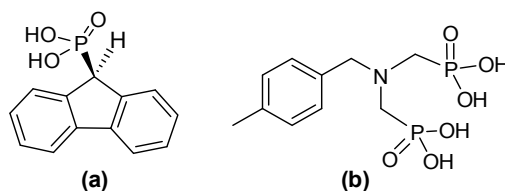
Among the hybrid materials, metal phosphonates represent a very large family that has been the object of numerous investigations [1] in view of various applications such as ion exchange properties [2], catalysis [3–7], luminescence [8–10], protonic conduction [11–14], or as a reservoir of bio-active metal ions [15,16]. Transition metal phosphonates have also been investigated for their attractive magnetic properties [17]. This is the case for Co(II) phosphonates, which can generate specific low-dimensional magnetic behavior, in connection with the high magnetic anisotropy of octahedral cobalt due to its spin–orbit coupling [18]. This is exemplified by several one-dimensional cobalt phosphonates with a ladder-like chain structure [19–25]. In those hybrids, the chains consist of isolated “Co₂” dimers of edge-shared CoO₆ octahedra connected through O–P–O bridges, causing them to be described by different authors as 1D antiferromagnets, with properties closely related to those of spin ladder systems. One-dimensional cobalt phosphonates with single chains built up of isolated CoO₅N octahedra or CoO₃N₂ trigonal bipyramids bridged by PO₃C tetrahedra were also obtained, showing weak magnetic interactions [26–28]. In contrast, the possibility to synthesize hybrid phosphonates involving isolated

infinite chains of corner-shared cobalt CoX_6 octahedra is quite rare. The compound $\text{Co}(\text{H}_2\text{L})(\text{H}_2\text{O})$, where $\text{L} = 4\text{-Me-C}_6\text{H}_4\text{-CH}_2\text{N}(\text{CPO}_3\text{H}_2)_2$, which consists of CoO_5N octahedra, is to our knowledge the only cobalt phosphonate to date that exhibits such a structural behavior [29,30]. Moreover, it has been shown to be a single-chain magnet (SCM), a magnetic behavior which has been the object of numerous investigations these last fifteen years [31–36] in view of its potential application in high-density data storage and quantum computing [37,38].

Based on these results, we believe that the investigation of one-dimensional $\text{Co}(\text{II})$ phosphonates is a challenging direction for the research of new magnetic properties. Bearing in mind that large molecular ligands in the phosphonate groups should allow the formation of isolated cobalt chains and control of the distances between them, we have thus embarked on the exploration of cobalt phosphonates prepared from 9-fluorenylphosphonic acid. We report herein a new phosphonate $\text{Co}(\text{H}_2\text{O})_2\text{PO}_3\text{C-C}_{12}\text{H}_9\cdot\text{H}_2\text{O}$, whose structure, built up of $\text{CoO}_4(\text{H}_2\text{O})_2$ octahedra, consists of isolated infinite perovskite-type $\text{Co}(\text{II})$ chains. We show that the latter exhibits 1D antiferromagnetic interactions and intra-chain spin canting, but, in spite of its structure closely related to that of $\text{Co}(\text{H}_2\text{L})(\text{H}_2\text{O})$ [29,30], is not an SCM.

2. Results and Discussion

The phosphonate $\text{Co}(\text{H}_2\text{O})_2\text{PO}_3\text{C-C}_{12}\text{H}_9\cdot\text{H}_2\text{O}$ was synthesized under hydrothermal conditions from cobalt(II) acetate $\text{Co}(\text{CH}_3\text{CO}_2)_2\cdot 4\text{H}_2\text{O}$, urea, and 9-fluorenylphosphonic acid ($\text{C}_{13}\text{H}_{11}\text{O}_3\text{P}$) (Scheme 1a). The use of urea in the hydrothermal synthesis allows slow basification of the pH media during the hydrolysis process of urea leading to an increase of the pH and to the fully deprotonated phosphonate function. The thermogravimetric analysis (TGA) and CHNS elemental analysis allowed the chemical formula of this compound to be established. Oblong-shaped crystallites (Figure 1) were identified in the homogenous batches of this compound by scanning electron microscopy (SEM), with an average length from 28 μm to 54.8 μm , width from 6 μm to 11.2 μm , and thickness of 0.8 μm . Energy-dispersive X-ray spectrometry (EDS) analysis, coupled with SEM, confirmed the result obtained by TGA, i.e., the molar ratio $\text{Co}/\text{P} = 1$.



Scheme 1. Chemical structure of organic precursors of hybrid materials: (a) 9-fluorenylphosphonic acid which is used in this study and (b) (4-methylphenyl)methylamine(bis-methylenephosphonic acid) which is used in the synthesis of cobalt-based single-chain magnets (SCMs) [30].

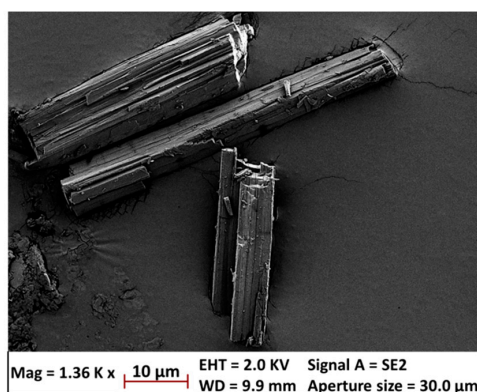


Figure 1. Oblong crystallites of $\text{Co}(\text{H}_2\text{O})_2\text{PO}_3\text{C-C}_{12}\text{H}_9\cdot\text{H}_2\text{O}$ observed by scanning electron microscopy.

2.1. Structural Study

Data were corrected from absorption using the *Twinabs* program [39] developed for scaling and corrections for twin and area detector data. The structure was determined using SIR2011 [40] and refined using the program *Jana 2006* [41]; the analysis of the electronic residue allows the location of all the missing atomic sites. Harmonic atomic displacement parameters were considered for Co, P, O, and C species. Hydrogen atoms were geometrically added; distance and angle restraints were introduced for H belonging to water molecules and these H were refined. Twin laws were introduced for the monoclinic phase and the ratio of the possible twin domains was refined. All the details of the refinement are summarized in Table 1. Atomic positions are listed in Table S1, thermal parameters in Table S2, bond angles in Table S3, and interatomic distances in Table S4. In order to check that the crystal is representative of the whole powder, a study by powder X-ray diffraction was performed. After analysis with *FullProf* software [1], a simulation of the pattern was realized. All the peaks were indexed and were shown to match with the $P2_1/c$ space group and lattice parameters found by single crystal X-ray diffraction (Figure S1, Supplementary Materials).

Table 1. Crystallographic data of $\text{Co}(\text{H}_2\text{O})_2\text{PO}_3\text{C}-\text{C}_{12}\text{H}_9\cdot\text{H}_2\text{O}$.

Formula	$\text{Co}(\text{H}_2\text{O})_2\text{PO}_3\text{C}-\text{C}_{12}\text{H}_9\cdot\text{H}_2\text{O}$
FW	357.20
Space group	$P2_1/c$
a (Å)	15.216(3)
b (Å)	4.827(8)
c (Å)	19.590(3)
α, β, γ (°)	90, 107.160(4), 90
Z	4
V (Å ³)	1375.0(4)
d_{calc} (g/cm ³)	1.716
μ (mm ⁻¹)	1.389
Radiation source λ (Å)	Mo K α 0.71069
Pattern range 2Θ (°)	2.8–66.94
No. of reflexions	21,476
No. of soft constraints	0
Weighted R factor	0.0877
$R[F^2 > 2\sigma(F^2)]$	0.0462
R_{int} (internal R -value)	0.0371
S (Goodness of the fit)	1.720

The view of the structure along b (Figure 2) shows that it consists of chains of $\text{CoO}_4(\text{H}_2\text{O})_2$ octahedra running along that direction. Two $\text{PO}_3\text{C}-\text{C}_{12}\text{H}_9$ groups are grafted on each cobalt chain in “*trans*” positions with respect to the chain, so that the cobalt chains and the fluorene groups form layers parallel to the (100) plane. Thus, in this structure, one single inorganic layer of cobalt chains alternates with a double organic layer of fluorene groups along a . Moreover, additional H_2O molecules are located in the inorganic layers between the cobalt chains. The arrangement of the cobalt polyhedra and PO_3C groups is better understood by considering the structure close to the a direction and by taking out the fluorene groups (Figure 3a). One observes that the cobalt [010] zig-zag chains consist of corner-sharing $\text{CoO}_4(\text{H}_2\text{O})_2$ octahedra with the perovskite-like geometry and can be formulated as $[\text{CoO}_3(\text{H}_2\text{O})_2]_{\infty}$. Each cobalt octahedron has its two free apical corners occupied by H_2O and shares two of its four equatorial O apices with the neighboring octahedra of the chain. The two remaining O apices of each octahedron are shared with the PO_3C tetrahedron linked to a fluorene group. In fact, each PO_3C group shares two corners with two $\text{CoO}_4(\text{H}_2\text{O})_2$ octahedra and one edge with another octahedron. The arrangement of the cobalt chains in the form of (100) layers can also be seen from the projection of the structure along c (Figure 4). This view shows that the fluorene groups “ $\text{C}_{12}\text{H}_{19}$ ” are directed along two transversal directions oriented at 40.13° and 42.93° with respect to the inorganic

layers. In one column, the fluorene moieties, with distance of 3.58 Å, are stacked along *c* in a face-to-face packing (Figure 2b). The interatomic Co–O and P–O distances (Table S4) are in agreement with the iono-covalent radii given by Shannon and Prewitt [42] and confirm the strong bonding of the structure along *b*. In contrast, laterally, within the inorganic layers, the linking between the chains along *c* is only ensured by hydrogen bonds between H₂O molecules and O atoms of the cobalt octahedral coordination environment and PO₃C tetrahedra (Figure 2a), whereas the cohesion of the structure between the layers, along *a*, is ensured by van der Waals interactions between the fluorene groups (orange dashed lines, Figure 4). The study of the Hirshfeld surface [43,44] and its corresponding two-dimensional fingerprint plots [45] of Co(H₂O)₂PO₃C–C₁₂H₉·H₂O are in good agreement with the above statements (Figure S2, Supplementary Materials). Indeed, the most numerous intermolecular interactions are the C···H contacts (38.6%) and H···H contacts (51.1%), which evidence for the main part C–H···π interactions between the fluorene moieties (Figure S2). These π···π interactions are known to play an important role in the cohesion of many aromatic phosphonate-containing materials structures [46–48]. The other contact types' contributions (P···C, C···O, C···C, and O···H) represent 10.3%.

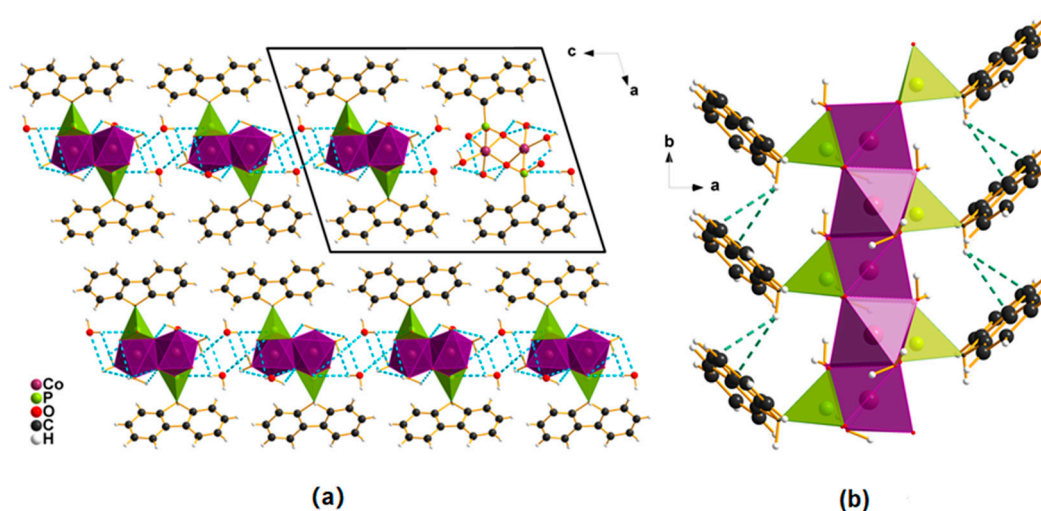


Figure 2. (a) Projection of the structure of Co(H₂O)₂PO₃C–C₁₂H₉·H₂O along the *b* axis. In blue dashed lines are represented the O–H···O hydrogen bonds between the H₂O molecules, oxygen atoms of the cobalt octahedra, and PO₃C tetrahedra, with H···O distances between 2.93 Å and 3.20 Å. The black square represents the unit cell. (b) Representation of one column along the *c* axis. The water molecules were removed in order to see clearly the π···π stacking between the fluorene moieties. The green dashed lines correspond to C–H···C interactions with H···C distances between 3.10 Å and 3.13 Å.

The structure of this phosphonate-based hybrid is very closely related to that of Co(H₂L)(H₂O), where L = 4-Me-C₆H₄-CH₂N(CPO₃H₂)₂ (Scheme 1b), previously described by Palić et al. [1,30]. The latter consists indeed of rather similar isolated chains of corner-sharing Co(II) octahedra (Figure 3b) interconnected through chains of phosphonate groups. However, the two types of chains differ by their geometry. In the present hybrid, the perovskite-type chains form Co–O–Co bond angles close to 180° (Figure 3a), whereas in the zig-zag chains of the Co(H₂L)(H₂O) compound (Figure 3b), two successive Co(II) octahedra are strongly tilted with respect to each other so that the Co–O–Co bond angles deviate largely from 180° (i.e., 122.09°). It will be shown further that such a different geometry may influence the magnetic properties of this phase.

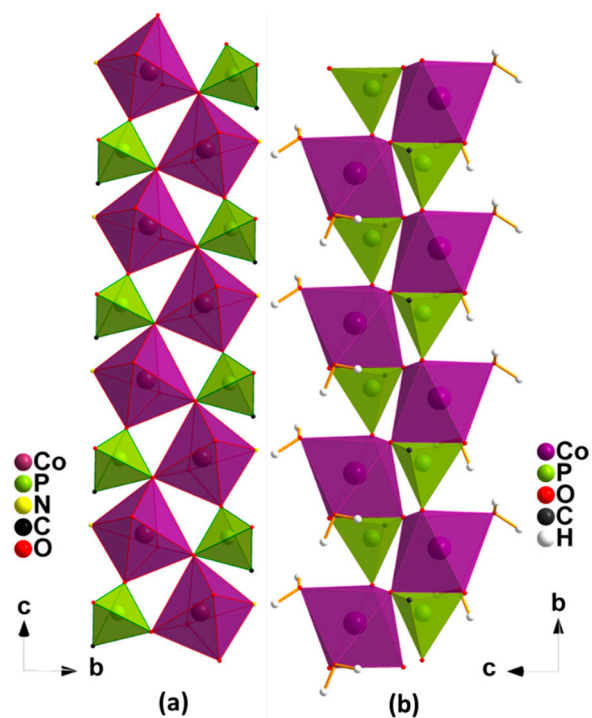


Figure 3. (a) Projection of the structure of $\text{Co}(\text{H}_2\text{O})_2\text{PO}_3\text{C}-\text{C}_{12}\text{H}_9\cdot\text{H}_2\text{O}$ along the *a* axis without fluorene groups; (b) Projection of $\text{Co}(\text{H}_2\text{L})(\text{H}_2\text{O})$ along the *a* axis without the organic part, adapted from the reference [30].

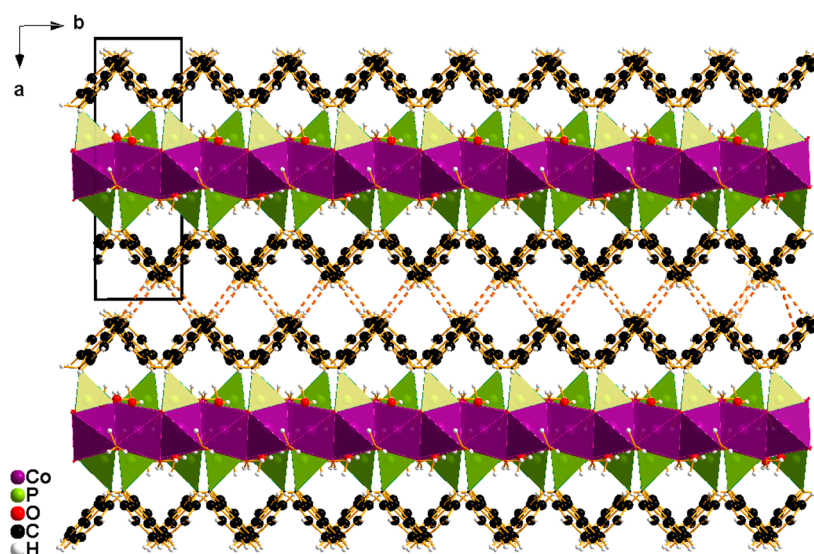


Figure 4. Projection of the structure of $\text{Co}(\text{H}_2\text{O})_2\text{PO}_3\text{C}-\text{C}_{12}\text{H}_9\cdot\text{H}_2\text{O}$ along the *c* axis. The black square represents the unit cell. The orange dashed lines correspond to C-H...C interactions between two organic layers with H...C distances between 2.90 Å and 3.20 Å.

2.2. Magnetic Properties

The temperature dependence of the molar magnetic susceptibility χ is presented Figure 5. The inverse of the susceptibility curve (inset Figure 5), shows a linear behavior between 200 K and 300 K. The latter can be fit above 200 K using the Curie–Weiss law $\chi = C/(T - \theta)$ which provides the Curie constant $C = 3.14 \text{ emu}\cdot\text{K}\cdot\text{mol}^{-1}$, in agreement with the expected value from the literature for six-coordinated “high-spin” Co(II) ($C = 2.8\text{--}3.4 \text{ emu}\cdot\text{K}\cdot\text{mol}^{-1}$) [49]. The experimental magnetic

moment deduced from the C value, $\mu_{\text{eff}} = 5.01 \mu_{\text{B}}$ (where μ_{B} is the Bohr magneton), is close to the calculated value of Co(II) , $\mu_{\text{eff}} = 5.20 \mu_{\text{B}}$, which has $[\text{Ar}]3d^7$ electronic configuration, implying a total spin S value of $3/2$ and a total angular momentum L of 3 . Note that the typical magnetic moments observed for octahedral complexes range from 4.7 to $5.2 \mu_{\text{B}}$ [49]. The Weiss temperature, $\theta = -9.93 \text{ K}$, suggests the presence of weak antiferromagnetic exchange interactions and/or spin–orbit coupling. This feature is corroborated by the variation of the product χT as a function of temperature, which shows a continuous decrease from $3.00 \text{ emu}\cdot\text{K}\cdot\text{mol}^{-1}$ at 300 K to $0.97 \text{ emu}\cdot\text{K}\cdot\text{mol}^{-1}$ at 5 K (Figure 5). The existence of such antiferromagnetic interactions is in agreement with the Kanamori–Goodenough rules for a 180° super exchange mechanism between Co(II) [50,51].

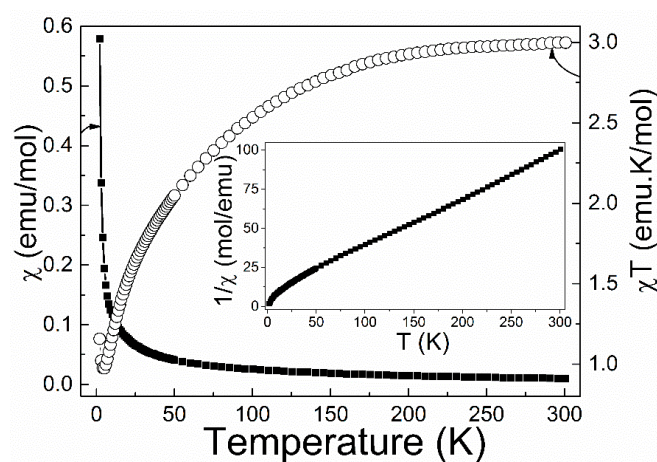


Figure 5. Variation of χ (black squares) and χT (open black circles) as function of the temperature for $\text{Co}(\text{H}_2\text{O})_2\text{PO}_3\text{C-C}_{12}\text{H}_9\cdot\text{H}_2\text{O}$ under 0.1 T .

When decreasing the temperature below 5 K , a small increase of χT can be observed, indicating some other magnetic contribution. This increase is observed in samples from different batches, indicating a likely intrinsic origin. In addition, the measurement of magnetization versus magnetic field at $T = 2 \text{ K}$ shows an S shape typical of spin canting (Figure 6).

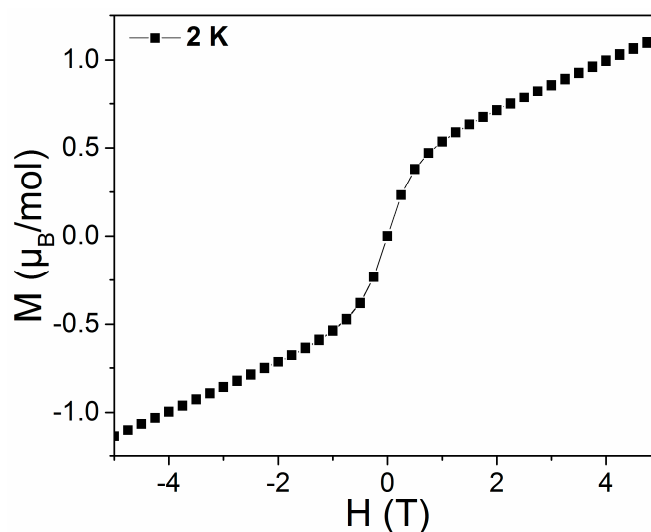


Figure 6. Variation of magnetization versus magnetic field at 2 K .

This Ising-like behaviour of the chains with spin canting at low temperature is similar to that of $\text{Co}(\text{H}_2\text{L})(\text{H}_2\text{O})$ [30]. Yet, contrarily to what is described for $\text{Co}(\text{H}_2\text{L})(\text{H}_2\text{O})$, we do not observe here

any hysteresis in the $M = f(H)$ curve. Moreover, measurement of alternating current (ac) susceptibility indicates that no slow relaxation process occurs within the temperature range 2 K–6 K and frequency range 0.1 Hz–1 kHz under a zero direct current (dc) field (Figure S3, Supplementary Materials). Note that the absence of single-chain magnetism was also emphasized in the one-dimensional Co(II) hydroxide $[\text{Co}_4(\text{phcina})_6(\text{OH})_2(\text{H}_2\text{O})_4] \cdot 2\text{H}_2\text{O}$ by Oka et al. [52] where single octahedral diamond chains are isolated from each other by 17 Å.

3. Experimental Section

Thermogravimetric analysis (TGA) was performed on polycrystalline samples using a SETARAM TAG 92 apparatus (SETARAM Instrumentation, Caluire, France) under an air atmosphere at the heating rate of 3 °C per minute from room temperature to 1000 °C. Scanning Electron Microscopy (SEM) characterization was performed with a Carl ZEISS SUPRA 55 (Carl Zeiss Microscopy GmbH, Jena, Germany) on a raw sample with gold metallization. Elemental analysis and atomic absorption testing were performed on a ThermoQuest NA2500 (THERMO FINNIGAN, Villebon sur Yvette, France) and on an Agilent Technologies 200 Series AA setup (Agilent Technologies, Les Ulis, France), respectively. Energy-dispersive X-ray spectrometry (EDS) analysis was performed with an EDAX analyzer (AMETEK Materials Analysis Division, Mahwah, NJ, USA). The magnetic susceptibility was recorded versus temperature with a SQUID Quantum Design magnetometer (Quantum Design, San Diego, CA, USA) operating in the temperature range from 2 K to 300 K according to Zero Field Cooling (ZFC) and Field Cooling (FC) procedures. The applied magnetic field was 0.1 T. For the alternated current (ac) susceptibility measurements, measurement was performed from 2 K to 6 K under the ac field of 0.05 T (linear regime) and the frequency range 0.1–1 KHz. A suitable single crystal of $\text{Co}(\text{H}_2\text{O})_2\text{PO}_3\text{C}-\text{C}_{12}\text{H}_9 \cdot \text{H}_2\text{O}$ was selected and an X-ray diffraction experiment was performed at room temperature using Mo $K\alpha$ radiation produced with a microfocus Incoatec 1μ sealed X-ray tube on a Kappa CCD diffractometer (Bruker, Billerica, MA., USA) equipped with an Apex2 CCD detector. Details of the data collection are summarized in Table 1 and in Tables S1–S4. On experimental frames for the highest θ area, a splitting of the reflections into four close spots is observed; the coupling between $K\alpha_1$ and $K\alpha_2$ radiations and the twin leads to a quadruplet of reflections typical for a twinning by reticular pseudo-merohedry. Plots of reciprocal lattice planes were assembled from the different scans; they provide an overall view of the reciprocal space useful both for the symmetry and for twin law analysis. The twin law compatible with the experiment is a π rotation around the c axis. Moreover, the conditions limiting the possible reflections are in agreement with the $P2_1/c$ space group ($h0l:l = 2n, 0k0:k = 2n$). *CrystalExplorer* software [53] was used to generate the Hirshfeld surface (HS) and the corresponding 2D fingerprint plots. The HSs were calculated on the fluorene moieties of the cobalt phosphonate in very high resolution with a standard void cluster mode (unit cell + 5 Å) and an isovalue of $0.002 \text{ e} \cdot \text{au}^{-3}$.

Crystallographic data have been deposited into the Cambridge Crystallographic Data Centre, with deposition numbers CCDC 1853487 for $\text{Co}(\text{H}_2\text{O})_2\text{PO}_3\text{C}-\text{C}_{12}\text{H}_9 \cdot \text{H}_2\text{O}$. These data can be obtained free of charge via www.ccdc.cam.ac.uk/conts/retrieving.html (or from the Cambridge Crystallographic Data Centre, 12 Union Road, Cambridge CB2 1EZ, UK; fax: (+44) 1223-336-033; or deposit@ccdc.ca.ac.uk).

3.1. Synthesis

All reagents were purchased from Sigma Aldrich (Saint-Quentin Fallavier, France) and Epsilon Chimie (Guipavas, France) and were used without prior purification in a hydrothermal synthesis process according to the following procedure: The $\text{Co}(\text{H}_2\text{O})_2(\text{PO}_3\text{C}-\text{C}_{12}\text{H}_9) \cdot \text{H}_2\text{O}$ phosphonate ($\text{CoPO}_6\text{C}_{13}\text{H}_{15}$, $M = 357.20 \text{ g/mol}$) was synthesized from an equimolar mixture of cobalt acetate tetrahydrated $\text{Co}(\text{C}_2\text{H}_3\text{O}_2)_2 \cdot 4\text{H}_2\text{O}$ (0.0506 g, 0.2 mmol), 9-fluorenyl-phosphonic acid $\text{C}_{13}\text{H}_{11}\text{O}_3\text{P}$ (0.0502 g, 0.2 mmol) (Scheme 1a), and urea $\text{N}_2\text{H}_4\text{CO}$ (0.0121 g, 0.2 mmol) dissolved in distilled water (15 mL) in a 20 mL polytetrafluoroethylene (PTFE) liner. Then, the liner was inserted in a Berghof DAB-2 digestive vessel and heated from room temperature to 140 °C over 20 h, maintained at 140 °C

for 30 h, and finally allowed to cool to room temperature within 20 h. After filtration, the final product, obtained as pink oblong-shaped crystals, was washed with distilled water, rinsed with ethanol, and then dried in air. The medium pH values before and after the hydrothermal process were 5.04 and 6.18, respectively. The chemical formula was confirmed by elemental analysis (found (calc.) C 43.26 (43.72), H 4.61 (4.23)) and by atomic absorption spectroscopy (found (theo.): $M(\text{Co})$ (g/mol) = 58.94 (58.93)).

3.2. Thermogravimetric Analysis

The thermogravimetric analysis (TGA) curve recorded on a polycrystalline sample (Figure 7) shows two weight losses between room temperature and 300 °C which are in good agreement with the departure of the three water molecules per $\text{Co}(\text{H}_2\text{O})_2\text{PO}_3\text{C}-\text{C}_{12}\text{H}_9\cdot\text{H}_2\text{O}$ formula (theoretical percentage of water: 15.13%). The dehydration process occurs in two steps: A first weight loss of 10.26% (theoretical value 10.1%) corresponding to the departure of two H_2O molecules between room temperature and 110 °C and a second weight loss of 4.85% from 110 °C to 300 °C corresponding to the departure of the last H_2O molecule (theoretical value 5%). Beyond 300 °C, the next weight losses are assigned to the ligand decomposition and to the transformation of the dehydrated compound into cobalt pyrophosphate $\text{Co}_2\text{P}_2\text{O}_7$. The composition and structure of the latter phase was confirmed by powder X-ray diffraction on the TGA residue (Figure S4, Supplementary Materials) and is in agreement with the total weight loss recorded by TGA (experimental value: 58.55%, theoretical value: 59.15%).

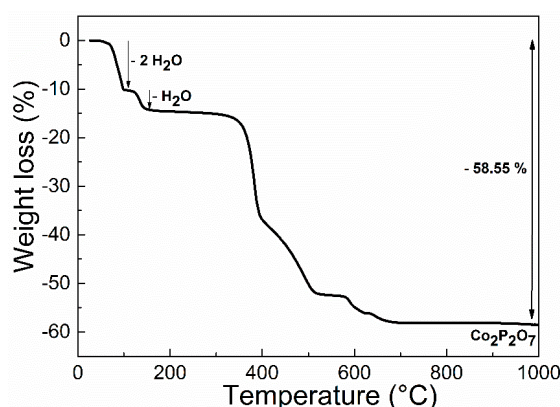


Figure 7. TGA curve of $\text{Co}(\text{H}_2\text{O})_2\text{PO}_3\text{C}-\text{C}_{12}\text{H}_9\cdot\text{H}_2\text{O}$ recorded in air from room temperature to 1000 °C.

4. Conclusions

A unique one-dimensional cobalt phosphonate that exhibits isolated perovskite-type chains of corner-sharing $\text{CoO}_4(\text{H}_2\text{O})_2$ octahedra was synthesized. The structure of this phosphonate is closely related to that of the compound $\text{Co}(\text{H}_2\text{L})(\text{H}_2\text{O})$, with $\text{L} = 4\text{-Me-C}_6\text{H}_4\text{-CH}_2\text{N}(\text{CPO}_3\text{H}_2)_2$, which similarly consists of chains of corner-sharing Co_5N octahedra. The magnetic behavior of this phase shows that, like the latter, it exhibits 1D antiferromagnetic interaction with possible spin canting at low temperature, but, in contrast, is not an SCM. This difference can be attributed to the different geometries of the octahedral chain in the two compounds and to the fact that weak antiferromagnetic interactions may appear between the chains in the present phosphonate. This study should foster further investigations of new 1D cobalt phosphonates, varying the nature of organic ligands in order to understand the magnetism of these compounds.

Supplementary Materials: The following are available online at <http://www.mdpi.com/2304-6740/6/3/93/s1>, Figure S1: X-ray diffraction data recorded on powder from $\text{Co}(\text{H}_2\text{O})_2\text{PO}_3\text{C}-\text{C}_{12}\text{H}_9\cdot\text{H}_2\text{O}$, Figure S2: (a) Hirshfeld Surface represented on the fluorene moiety of $\text{Co}(\text{H}_2\text{O})_2\text{PO}_3\text{C}-\text{C}_{12}\text{H}_9\cdot\text{H}_2\text{O}$ with a shape index mapping; (b) Representation of the corresponding two-dimensional fingerprint plot showing the contribution of each contact-type in percentage, Figure S3: Representation of the AC susceptibility of $\text{Co}(\text{H}_2\text{O})_2\text{PO}_3\text{C}-\text{C}_{12}\text{H}_9\cdot\text{H}_2\text{O}$, Figure S4: X-ray diffraction data recorded on the TGA residue of $\text{Co}(\text{H}_2\text{O})_2\text{PO}_3\text{C}-\text{C}_{12}\text{H}_9\cdot\text{H}_2\text{O}$, Tables S1–S4:

Atomic positions, thermal parameters, bond angles, and interatomic distances of $\text{Co}(\text{H}_2\text{O})_2\text{PO}_3\text{C}-\text{C}_{12}\text{H}_9\cdot\text{H}_2\text{O}$, Cif and Check cif files of $\text{Co}(\text{H}_2\text{O})_2\text{PO}_3\text{C}-\text{C}_{12}\text{H}_9\cdot\text{H}_2\text{O}$.

Author Contributions: Conceptualization, J.-M.R., C.B., and B.R.; Validation, all authors; Formal Analysis, A.P., O.P., C.B., V.C., J.-M.R.; Writing—Original Draft Preparation, B.R., C.B.; Writing—Review & Editing, all authors equally contributed; Visualization, C.B.; Project Administration, G.R., P.-A.J., J.-M.R.; Funding Acquisition, G.R., P.-A.J., J.-M.R.

Funding: This research was funded by the Agence Nationale de la Recherche, grant number [ANR-14-CE07-0004-01 (HYMN)].

Acknowledgments: We thank the Agence Nationale de la Recherche (Contract No ANR-14-CE07-0004-01 (HYMN)) for financial support. The authors also express their grateful acknowledgment of technical support from Sylvie Collin and Fabien Veillon from the CRISMAT laboratory.

Conflicts of Interest: The authors declare no conflict of interest.

References

1. Clearfield, A.; Demadis, K. *Metal Phosphonate Chemistry: From Synthesis to Applications*; Royal Society of Chemistry: Cambridge, UK, 2011; ISBN 978-1-84973-356-4.
2. Silbernagel, R.; Martin, C.H.; Clearfield, A. Zirconium(IV) Phosphonate-Phosphates as Efficient Ion-Exchange Materials. *Inorg. Chem.* **2016**, *55*, 1651–1656. [[CrossRef](#)] [[PubMed](#)]
3. Song, J.; Zhou, B.; Zhou, H.; Wu, L.; Meng, Q.; Liu, Z.; Han, B. Porous Zirconium–Phytic Acid Hybrid: A Highly Efficient Catalyst for Meerwein–Ponndorf–Verley Reductions. *Angew. Chem. Int. Ed.* **2015**, *54*, 9399–9403. [[CrossRef](#)] [[PubMed](#)]
4. Hu, A.; Yee, G.T.; Lin, W. Magnetically Recoverable Chiral Catalysts Immobilized on Magnetite Nanoparticles for Asymmetric Hydrogenation of Aromatic Ketones. *J. Am. Chem. Soc.* **2005**, *127*, 12486–12487. [[CrossRef](#)] [[PubMed](#)]
5. Wang, Z.; Heising, J.M.; Clearfield, A. Sulfonated Microporous Organic–Inorganic Hybrids as Strong Bronsted Acids. *J. Am. Chem. Soc.* **2003**, *125*, 10375–10383. [[CrossRef](#)] [[PubMed](#)]
6. Hu, A.; Ngo, H.L.; Lin, W. Chiral Porous Hybrid Solids for Practical Heterogeneous Asymmetric Hydrogenation of Aromatic Ketones. *J. Am. Chem. Soc.* **2003**, *125*, 11490–11491. [[CrossRef](#)] [[PubMed](#)]
7. Maillet, C.; Janvier, P.; Pipelier, M.; Praveen, T.; Andres, Y.; Bujoli, B. Hybrid Materials for Catalysis? Design of New Phosphonate-Based Supported Catalysts for the Hydrogenation of Ketones under Hydrogen Pressure. *Chem. Mater.* **2001**, *13*, 2879–2884. [[CrossRef](#)]
8. Mao, J.-G. Structures and luminescent properties of lanthanide phosphonates. *Coord. Chem. Rev.* **2007**, *251*, 1493–1520. [[CrossRef](#)]
9. Rueff, J.-M.; Barrier, N.; Boudin, S.; Dorcet, V.; Caignaert, V.; Boullay, P.; Hix, G.B.; Jaffrès, P.-A. Remarkable thermal stability of Eu(4-phosphonobenzoate): Structure investigations and luminescence properties. *Dalton Trans.* **2009**, 10614–10620. [[CrossRef](#)] [[PubMed](#)]
10. Mutelet, B.; Boudin, S.; Pérez, O.; Rueff, J.M.; Labbé, C.; Jaffrès, P.A. $\text{La}_{1-x}\text{Ln}_x\text{H}(\text{O}_3\text{PCH}_3)_2$ (Ln = Tb, Eu; $0 < x \leq 1$): An organic-inorganic hybrid with lanthanide chains and tunable luminescence properties. *Dalton Trans.* **2015**, *44*, 1186–1192. [[CrossRef](#)] [[PubMed](#)]
11. Colodrero, R.M.P.; Olivera-Pastor, P.; Losilla, E.R.; Aranda, M.A.G.; Leon-Reina, L.; Papadaki, M.; McKinlay, A.C.; Morris, R.E.; Demadis, K.D.; Cabeza, A. Multifunctional lanthanum tetrakisphosphonates: Flexible, ultramicroporous and proton-conducting hybrid frameworks. *Dalton Trans.* **2012**, *41*, 4045–4051. [[CrossRef](#)] [[PubMed](#)]
12. Horike, S.; Umeyama, D.; Kitagawa, S. Ion Conductivity and Transport by Porous Coordination Polymers and Metal–Organic Frameworks. *Acc. Chem. Res.* **2013**, *46*, 2376–2384. [[CrossRef](#)] [[PubMed](#)]
13. Kim, S.; Dawson, K.W.; Gelfand, B.S.; Taylor, J.M.; Shimizu, G.K.H. Enhancing Proton Conduction in a Metal–Organic Framework by Isomorphous Ligand Replacement. *J. Am. Chem. Soc.* **2013**, *135*, 963–966. [[CrossRef](#)] [[PubMed](#)]
14. Donnadio, A.; Nocchetti, M.; Costantino, F.; Taddei, M.; Casciola, M.; da Silva Lisboa, F.; Vivani, R. A layered mixed zirconium phosphate/phosphonate with exposed carboxylic and phosphonic groups: X-ray powder structure and proton conductivity properties. *Inorg. Chem.* **2014**, *53*, 13220–13226. [[CrossRef](#)] [[PubMed](#)]

15. Berchel, M.; Gall, T.L.; Denis, C.; Hir, S.L.; Quentel, F.; Elléouet, C.; Montier, T.; Rueff, J.-M.; Salaün, J.-Y.; Haelters, J.-P.; et al. A silver-based metal–organic framework material as a ‘reservoir’ of bactericidal metal ions. *New J. Chem.* **2011**, *35*, 1000–1003. [[CrossRef](#)]
16. Rueff, J.-M.; Perez, O.; Caignaert, V.; Hix, G.; Berchel, M.; Quentel, F.; Jaffrès, P.-A. Silver-Based Hybrid Materials from meta- or para-Phosphonobenzoic Acid: Influence of the Topology on Silver Release in Water. *Inorg. Chem.* **2015**, *54*, 2152–2159. [[CrossRef](#)] [[PubMed](#)]
17. Bao, S.-S.; Zheng, L.-M. Magnetic materials based on 3d metal phosphonates. *Coord. Chem. Rev.* **2016**, *319*, 63–85. [[CrossRef](#)]
18. Zheng, L.-M.; Duan, Y. Structural and Magnetic Studies of Cobalt Phosphonates. In *Metal Phosphonate Chemistry*; Clearfield, A., Demadis, K., Eds.; Royal Society of Chemistry: Cambridge, UK, 2011; Chapter 8; pp. 235–278. ISBN 978-1-84973-356-4.
19. Yin, P.; Gao, S.; Zheng, L.-M. Xin Magnetic Properties of Metal Diphosphonate Compounds with One-Dimensional Chain Structures. *Chem. Mater.* **2003**, *15*, 3233–3236. [[CrossRef](#)]
20. Zheng, L.-M.; Gao, S.; Yin, P. Xin One-Dimensional Cobalt Diphosphonates Exhibiting Weak Ferromagnetism and Field-Induced Magnetic Transitions. *Inorg. Chem.* **2004**, *43*, 2151–2156. [[CrossRef](#)] [[PubMed](#)]
21. Yin, P.; Gao, S.; Wang, Z.-M.; Yan, C.-H.; Zheng, L.-M. Xin Field-Induced Magnetic Transitions in Metal Phosphonates with Ladderlike Chain Structures: $(\text{NH}_3\text{C}_6\text{H}_4\text{NH}_3)_2\text{M}_2(\text{hedpH})_2 \cdot \text{H}_2\text{O}$ [M = Fe, Co, Mn, Zn; hedp = C(CH₃)(OH)(PO₃)₂]. *Inorg. Chem.* **2005**, *44*, 2761–2765. [[CrossRef](#)] [[PubMed](#)]
22. Zhang, Z.-C.; Bao, S.-S.; Zheng, L.-M. Ladder-like metal diphosphonates exhibiting field-induced magnetic transitions. *Inorg. Chem. Commun.* **2007**, *10*, 1063–1066. [[CrossRef](#)]
23. Zhang, Z.-C.; Gao, S.; Zheng, L.-M. Cobalt diphosphonate with a new double chain structure exhibiting field-induced magnetic transition. *Dalton Trans.* **2007**, 4681–4684. [[CrossRef](#)] [[PubMed](#)]
24. Yang, T.-H.; Knowles, E.S.; Pajerowski, D.M.; Xia, J.-S.; Yin, L.; Gao, S.; Meisel, M.W.; Zheng, L.-M. Metal Monophosphonates $\text{M}\{(2\text{-C}_5\text{H}_4\text{NO})\text{CH}_2\text{PO}_3\}(\text{H}_2\text{O})_2$ (M = Co, Ni, Mn, Cd): Synthesis, Structure, and Magnetism. *Inorg. Chem.* **2010**, *49*, 8474–8480. [[CrossRef](#)] [[PubMed](#)]
25. Yang, Y.; Chen, M.; Tang, X.; Yuan, R.; Ma, Y. A one-dimensional cobalt phosphonate showing field-induced magnetic transition. *Inorg. Chem. Commun.* **2018**, *89*, 60–63. [[CrossRef](#)]
26. Wang, P.; Duan, Y.; Zheng, L. One-dimensional metal phosphonates based on 6-phosphononicotinic acid: A structural and magnetic study. *Sci. China Chem.* **2010**, *53*, 2112–2117. [[CrossRef](#)]
27. Cao, D.-K.; Xiao, J.; Li, Y.-Z.; Clemente-Juan, J.M.; Coronado, E.; Zheng, L.-M. Metal Phosphonates Based on $\{[(\text{Benzimidazol-2-ylmethyl})\text{imino}]\text{bis}(\text{methylene})\text{bis}(\text{phosphonic Acid})\}$: Syntheses, Structures and Magnetic Properties of the Chain Compounds $[\text{M}\{(\text{C}_7\text{H}_5\text{N}_2)\text{CH}_2\text{N}(\text{CH}_2\text{PO}_3\text{H}_2)\}]$ (M = Mn, Fe, Co, Cu, Cd). *Eur. J. Inorg. Chem.* **2006**, *2006*, 1830–1837. [[CrossRef](#)]
28. Han, G.-F.; Luo, H.-Z.; Ye, Q.; Xiong, R.-G. Two Novel Cobalt(II) Coordination Polymers Based on the Herbicide Glyphosate as a Building Block and their Magnetic Properties. *Z. Anorg. Allg. Chem.* **2008**, *634*, 1991–1995. [[CrossRef](#)]
29. Sun, Z.-M.; Prosvirin, A.V.; Zhao, H.-H.; Mao, J.-G.; Dunbar, K.R. New type of single chain magnet based on spin canting in an antiferromagnetically coupled Co(II) chain. *J. Appl. Phys.* **2005**, *97*, 10B305. [[CrossRef](#)]
30. Pali, A.V.; Ostrovsky, S.M.; Klokishner, S.I.; Reu, O.S.; Sun, Z.-M.; Prosvirin, A.V.; Zhao, H.-H.; Mao, J.-G.; Dunbar, K.R. Origin of the Single Chain Magnet Behavior of the $\text{Co}(\text{H}_2\text{L})(\text{H}_2\text{O})$ Compound with a 1D Structure. *J. Phys. Chem. A* **2006**, *110*, 14003–14012. [[CrossRef](#)] [[PubMed](#)]
31. Caneschi, A.; Gatteschi, D.; Lalioti, N.; Sangregorio, C.; Sessoli, R.; Venturi, G.; Vindigni, A.; Rettori, A.; Pini, M.G.; Novak, M.A. Cobalt(II)-Nitronyl Nitroxide Chains as Molecular Magnetic Nanowires. *Angew. Chem. Int. Ed.* **2001**, *40*, 1760–1763. [[CrossRef](#)]
32. Caneschi, A.; Gatteschi, D.; Lalioti, N.; Sessoli, R.; Sorace, L.; Tangoulis, V.; Vindigni, A. Ising-Type Magnetic Anisotropy in a Cobalt(II) Nitronyl Nitroxide Compound: A Key to Understanding the Formation of Molecular Magnetic Nanowires. *Chem. Eur. J.* **2002**, *8*, 286–292. [[CrossRef](#)]
33. Clérac, R.; Miyasaka, H.; Yamashita, M.; Coulon, C. Evidence for Single-Chain Magnet Behavior in a $\text{Mn}^{\text{III}}\text{–Ni}^{\text{II}}$ Chain Designed with High Spin Magnetic Units: A Route to High Temperature Metastable Magnets. *J. Am. Chem. Soc.* **2002**, *124*, 12837–12844. [[CrossRef](#)] [[PubMed](#)]
34. Lescouëzec, R.; Vaissermann, J.; Ruiz-Pérez, C.; Lloret, F.; Carrasco, R.; Julve, M.; Verdaguer, M.; Dromzee, Y.; Gatteschi, D.; Wernsdorfer, W. Cyanide-Bridged Iron(III)–Cobalt(II) Double Zigzag Ferromagnetic Chains: Two New Molecular Magnetic Nanowires. *Angew. Chem.* **2003**, *115*, 1521–1524. [[CrossRef](#)]

35. Miyasaka, H.; Clérac, R.; Mizushima, K.; Sugiura, K.; Yamashita, M.; Wernsdorfer, W.; Coulon, C. $[3\text{Mn}_2(\text{saltmen})_2\text{Ni}(\text{pao})_2(\text{L})_2](\text{A})_2$ with L = Pyridine, 4-Picoline, 4-*tert*-Butylpyridine, N-Methylimidazole and A = ClO_4^- , BF_4^- , PF_6^- , ReO_4^- : A Family of Single-Chain Magnets. *Inorg. Chem.* **2003**, *42*, 8203–8213. [[CrossRef](#)] [[PubMed](#)]
36. Coulon, C.; Clérac, R.; Lecren, L.; Wernsdorfer, W.; Miyasaka, H. Glauber dynamics in a single-chain magnet: From theory to real systems. *Phys. Rev. B* **2004**, *69*, 132408. [[CrossRef](#)]
37. Gatteschi, D.; Sessoli, R. Quantum Tunneling of Magnetization and Related Phenomena in Molecular Materials. *Angew. Chem. Int. Ed.* **2003**, *42*, 268–297. [[CrossRef](#)] [[PubMed](#)]
38. Gatteschi, D.; Sessoli, R.; Villain, J. Mesoscopic Physics and Nanotechnology. In *Molecular Nanomagnets*; Oxford University Press: Oxford, UK, 2006; ISBN 978-0-19-856753-0.
39. Sheldrick, G.M. *Twinabs*; University of Göttingen: Göttingen, Germany, 1996.
40. Burla, M.C.; Caliandro, R.; Camalli, M.; Carrozzini, B.; Cascarano, G.L.; Giacovazzo, C.; Mallamo, M.; Mazzone, A.; Polidori, G.; Spagna, R. *SIR2011*: A new package for crystal structure determination and refinement. *J. Appl. Crystallogr.* **2012**, *45*, 357–361. [[CrossRef](#)]
41. Václav, P.; Michal, D.; Lukáš, P. Crystallographic Computing System JANA2006: General features. *zkri* **2014**, *229*, 345. [[CrossRef](#)]
42. Shannon, R.D.; Prewitt, C.T. Effective ionic radii in oxides and fluorides. *Acta Crystallogr. Sect. B Struct. Crystallogr. Cryst. Chem.* **1969**, *25*, 925–946. [[CrossRef](#)]
43. Spackman, M.A.; Jayatilaka, D. Hirshfeld surface analysis. *CrystEngComm* **2009**, *11*, 19–32. [[CrossRef](#)]
44. McKinnon, J.J.; Spackman, M.A.; Mitchell, A.S. Novel tools for visualizing and exploring intermolecular interactions in molecular crystals. *Acta Crystallogr. Sect. B* **2004**, *60*, 627–668. [[CrossRef](#)] [[PubMed](#)]
45. Spackman, M.A.; McKinnon, J.J. Fingerprinting intermolecular interactions in molecular crystals. *CrystEngComm* **2002**, *4*, 378–392. [[CrossRef](#)]
46. Bloyet, C.; Rueff, J.-M.; Caignaert, V.; Lohier, J.-F.; Cardin, J.; Jaffrès, P.-A.; Raveau, B. Fluorenyl Zinc Phosphonate $\text{Zn}(\text{H}_2\text{O})\text{PO}_3\text{-C}_{13}\text{H}_9\cdot\text{H}_2\text{O}$: Hybrid Columnar Structure with Strong C–H $\cdots\pi$ Interactions. *Z. Anorg. Allg. Chem.* **2017**, *643*, 250–255. [[CrossRef](#)]
47. Demadis, K.D.; Panera, A.; Anagnostou, Z.; Varouhas, D.; Kirillov, A.M.; Čísařová, I. Disruption of “Coordination Polymer” Architecture in Cu^{2+} Bis-Phosphonates and Carboxyphosphonates by Use of 2,2'-Bipyridine as Auxiliary Ligand: Structural Variability and Topological Analysis. *Cryst. Growth Des.* **2013**, *13*, 4480–4489. [[CrossRef](#)]
48. Bloyet, C.; Rueff, J.-M.; Cardin, J.; Caignaert, V.; Doualan, J.-L.; Lohier, J.-F.; Jaffrès, P.-A.; Raveau, B. Excimer and Red Luminescence Due to Aggregation-Induced Emission in Naphthalene Based Zinc Phosphonate. *Eur. J. Inorg. Chem.* **2018**, 3095–3103. [[CrossRef](#)]
49. Carlin, R.L. *Magnetochemistry*; Springer: Berlin/Heidelberg, Germany, 1986; ISBN 978-3-642-70735-3.
50. Goodenough, J.B. An interpretation of the magnetic properties of the perovskite-type mixed crystals $\text{La}_{1-x}\text{Sr}_x\text{CoO}_{3-\lambda}$. *J. Phys. Chem. Solids* **1958**, *6*, 287–297. [[CrossRef](#)]
51. Kanamori, J. Superexchange interaction and symmetry properties of electron orbitals. *J. Phys. Chem. Solids* **1959**, *10*, 87–98. [[CrossRef](#)]
52. Oka, Y.; Inoue, K.; Kumagai, H.; Kurmoo, M. Long-Range Magnetic Ordering at 5.5 K for Cobalt(II)–Hydroxide Diamond Chains Isolated by 17 Å with α -Phenylcinamate. *Inorg. Chem.* **2013**, *52*, 2142–2149. [[CrossRef](#)] [[PubMed](#)]
53. Wolff, S.K.; Grimwood, D.J.; McKinnon, J.J.; Turner, M.J.; Jayatilaka, D.; Spackman, M.A. *CrystalExplorer*; University of Western Australia: Crawley, WA, Australia, 2012.

